Substructure of Direction-Selective Receptive Fields in Macaque V1

Margaret S. Livingstone and Bevil R. Conway

J Neurophysiol 89:2743-2759, 2003. doi:10.1152/jn.00822.2002

Journal of Neurophysiology publishes original articles on the function of the nervous system. It is published 12 times a year (monthly) by the American Physiological Society, 9650 Rockville Pike, Bethesda MD 20814-3991. ISSN: 0022-3077, ESSN: 1522-1598. Visit our website at http://www.the-aps.org/.

J Neurophysiol 89: 2743–2759, 2003;
10.1152/jn.00822.2002.

Substructure of Direction-Selective Receptive Fields in Macaque V1

Margaret S. Livingstone and Bevil R. Conway
Department of Neurobiology, Harvard Medical School, Boston, Massachusetts 02115

Submitted 17 September 2002; accepted in final form 26 December 2002

Livingstone, Margaret S. and Bevil R. Conway. Substructure of direction-selective receptive fields in macaque V1. *J Neurophysiol* 89: 2743–2759, 2003; 10.1152/jn.00822.2002. We used two-dimensional (2-D) sparse noise to map simultaneous and sequential two-spot interactions in simple and complex direction-selective cells in macaque V1. Sequential-interaction maps for both simple and complex cells showed preferred-direction facilitation and null-direction suppression for same-contrast stimulus sequences and the reverse for inverting-contrast sequences, although the magnitudes of the interactions were weaker for the simple cells. Contrast-sign selectivity in complex cells indicates that direction-selective interactions in these cells must occur in antecedent simple cells or in simple-cell-like dendritic compartments. Our maps suggest that direction selectivity, and ON and OFF segregation perpendicular to the orientation axis, can occur prior to receptive-field elongation along the orientation axis. 2-D interaction maps for some complex cells showed elongated alternating facilitatory and suppressive interactions as predicted if their inputs were orientation-selective simple cells. The negative interactions, however, were less elongated than the positive interactions, and there was an inflection at the origin in the positive interactions, so the interactions were chevron-shaped rather than band-like. Other complex cells showed only two round interaction regions, one negative and one positive. Several explanations for the map shapes are considered, including the possibility that directional interactions are generated directly from unoriented inputs.

INTRODUCTION

Forty years ago it was proposed that complex cells are generated by combining the inputs from several simple cells, which themselves are generated from several spatially aligned lateral geniculate (LGN) inputs (Hubel and Wiesel 1962). Hubel and Wiesel proposed this hierarchy to explain their observation that even though both simple and complex cells show orientation selectivity, only simple cells have an oriented structure to their receptive fields. Both simple and complex cells can show many kinds of response selectivity, such as orientation tuning, spatial frequency tuning, color selectivity, disparity tuning, or direction selectivity; in general, these selectivities are apparent in simple-cell receptive-field structure but not in complex-cell receptive-field organization. This difference is consistent with the idea that the selectivities of complex cells are generated at an antecedent simple-cell stage. But evidence that complex cells are generated by combining simple cells has been difficult to come by (for review see Alonso et al. 2001). Indeed, some complex cells do receive direct geniculate inputs (Bullier and Henry 1979; Ferster and Lindstrom 1983; Hoffman and Stone 1971; Martin and Whitteridge 1984; Tanaka 1983), leaving open the possibility that complex cells may not require an antecedent simple-cell stage (Mel et al. 1998). None of these studies, however, deal with directional cells, which can be both simple and complex (Goodwin and Henry 1975; Schiller et al. 1976). Whether directional complex cells, in particular, are built up from directional simple cells is an open question, and one that we address here.

The question of how complex-cell response selectivity, including directionality, is generated can be approached by looking at responses of complex cells to pairs of stimuli (Barlow and Levick 1965; Livingstone et al. 2001; Movshon et al. 1978b; Rybicki et al. 1972; Szulborski and Palmer 1990). That is, if selectivity is not apparent in receptive-field maps (1st-order maps) made using independently presented single stimuli, it may be apparent in maps showing interactions between responses to pairs of stimuli (2nd-order maps); direction selectivity is apparent as interactions between sequential stimuli. (The *interaction* between responses to a pair of stimuli is the paired-stimulus response minus the sum of the responses to the 2 stimuli presented independently.) In complex cells, paired-stimulus interactions can show substructure that resembles simple-cell receptive fields (Rybicki et al. 1972; Movshon et al. 1978b; Szulborski and Palmer 1990). This substructure has been interpreted as revealing the receptive-field organization of antecedent cells (i.e. simple cells) but need not (Emerson et al. 1987). Interaction maps generated from complex cells using pairs of bars have shown substructure for spatial frequency (Movshon et al. 1978b), direction selectivity (Baker 2001; Conway and Livingstone 2002; Emerson et al. 1987, 1992), and disparity tuning (Anzai et al. 1999; Livingstone and Tsao 1999; Ohzawa et al. 1990).

The preceding studies all used bar stimuli, oriented parallel to the cells' preferred orientation, so the interactions were mapped in only one spatial dimension—the dimension perpendicular to the preferred orientation. This approach assumes that interactions are homogeneous in the dimension parallel to the preferred orientation, an assumption that has been supported by the few studies mapping interactions in two spatial dimensions (Gaska et al. 1994; Szulborski and Palmer 1990).

In a delightful paper, Szulborski and Palmer (1990) used two-dimensional sparse white noise to map *simultaneous* interactions between pairs of small bar and square stimuli in nondirectional complex cells in the cat. The interaction maps revealed elongated parallel bands of alternating facilitatory and suppressive interactions, consistent with the hypothesis that the

Address reprint requests to M. Livingstone (E-mail: mlivingstone@hms.harvard.edu).

The costs of publication of this article were defrayed in part by the payment of page charges. The article must therefore be hereby marked "*advertisement*" in accordance with 18 U.S.C. Section 1734 solely to indicate this fact.

orientation selectivity of complex cells is inherited from antecedent simple cells. Gaska et al. (1994) used two-dimensional (2-D) white noise to estimate the second-order maps for complex cells in macaque V1. They found that, as in the cat, nondirectional complex cells showed parallel bands of interactions, elongated parallel to the cells' preferred orientation. They also found similar elongated parallel bands in direction-selective cells, and the location of these alternating bands of facilitatory and suppressive interactions shifted when they looked at sequential interactions in a manner consistent with the cell's direction selectivity. Livingstone et al. (2001) showed that even in an extrastriate area, MT, with its huge receptive fields, paired-stimulus 2-D directional interactions were very local and contrast-sign specific. However, the interactions in MT cells did not necessarily form elongated parallel bands, as previously described in V1 (Gaska et al. 1994), but were, instead, often crescent, or chevron, shaped. Because MT cells exhibited a subtle but critical deviation from what would be predicted if directional interactions are generated at a simple-cell stage, we sought to readdress the structure of the 2-D directional interactions in macaque V1.

METHODS

We mapped 2-D paired-stimulus interactions in 73 complex cells and 34 simple cells in primary visual cortex (V1) of three alert fixating macaque monkeys. The monkeys were prepared for chronic recording under general anesthesia using sterile techniques (Livingstone 1998). The monkeys were trained to keep their gaze within 1° of a small spot to receive a juice reward. Spikes were used for mapping only if the monkey's eyes were within the fixation window at the time of stimulus onset. Eye position was determined with a scleral eye coil monitored in a magnetic-field coil (CNC Engineering, Seattle, WA). The eye monitor has a spatial resolution of 0.05° (without the monkey) and was calibrated at the beginning of each recording session by having the monkeys look in random order at the center of the monitor and at four dots at the corners of the monitor. The monkeys had to maintain fixation for 2–4 s within the fixation window to receive a juice reward. During periods of stable fixation, the average standard deviation of the eye position was 0.1°. Receptive-field eccentricities were either between 2 and 5° (for cells recorded on the opercular surface) or between 10 and 25° (for cells recorded in the roof of the calcarine sulcus).

Neuronal responses were recorded extracellularly using fine electropolished tungsten electrodes coated with vinyl lacquer (Frederick Haer, Bowdoinham, ME) (Hubel 1957). Units were isolated using a dual-window discriminator (BAK Electronics, Germantown, MD) after they were amplified and band-pass filtered (1–10 kHz). Only well-isolated single units were analyzed.

Cortical cells were screened for direction-selectivity using optimally oriented bars that were swept across the center of the cells' receptive fields. Cells were tested with both light and dark bars (on a gray background). A direction index (DI) was calculated from the responses to moving bars: $DI = (R_p - R_n)/(R_p + R_n)$, where R_p is the response in the preferred direction and R_n is the response in the null direction. Cells that gave a 50% greater response to movement of the bar in one direction over movement of the bar in the opposite direction ($DI > 0.2$), for either contrast bar, and did not show opposite direction preference for light and dark bars were accepted as direction selective.

2-D interaction maps

The 2-D mapping stimulus, diagrammed in Fig. 1, *A* and *B*, consisted of pairs of small squares (0.15° for cells with receptive-field eccentricities less than 5°; 0.3° for cells at 10–25° eccentricity). The stimuli were presented at 75 Hz, with two squares presented each frame (13 ms) at random positions within a square stimulus range just larger than the cell's activating region. The pixel position of the squares was random, not in a stimulus-scaled grid. For the same-minus-inverting maps (see following text), each frame consisted of one white and one black square; for the same-contrast maps (see following text), two squares of the same contrast were presented each frame. For all stimulus conditions, we used three levels of luminance, black, gray, and white, in which the white-and-black stimuli were 19 cd/m^2 above and below the mean gray background luminance of 20

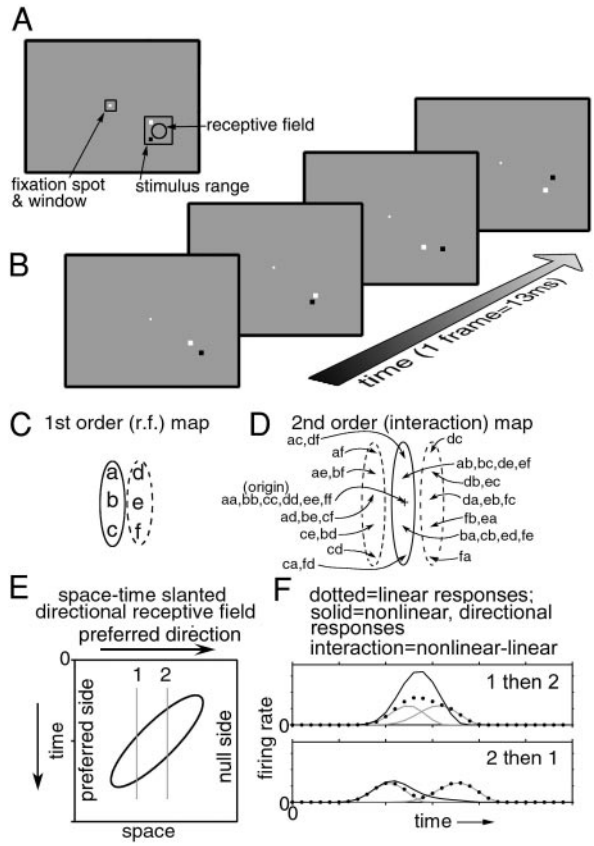

FIG. 1. *A* and *B*: stimulus configuration used to generate 2-dimensional (2-D) interaction maps (not to scale). While the monkey fixated, small square stimuli were presented at 75 Hz at random positions within a stimulus range just larger than the cell's activating region. In each frame, 2 stimuli were presented. For the experiments in Figs. 2–7, the 2 stimuli were always 1 black and 1 white. For the experiments in Fig. 8, the 2 stimuli were always both white or both black. Spikes were reverse correlated with the difference in position of pairs of stimuli, in either the same or previous frames. *C*: idealized 1st-order, space/space map for a simple cell; solid lines enclose an ON subregion and dotted lines enclose an OFF subregion. *D*: the predicted interaction patterns arising between and within each of the locations indicated in *C*. Solid lines outline same-contrast facilitatory interactions, and dotted lines outline same-contrast suppressive interactions. The stimulus-position pairs that map to each point in the interaction map are indicated as letter pairs, corresponding to probe (1st letter) and reference (2nd letter) stimulus pairs at the receptive-field locations indicated. *E*: idealized space-time map of a directional simple cell. *F*: facilitatory and suppressive interactions between 2 responses. Responses to each stimulus, presented at position 1 or 2 in *E*, alone are shown in gray. For each sequential stimulus pair, the linear sum of the 2 responses is shown by a dotted line. For this linear sum the response in the preferred direction will reach a higher peak firing rate than the response to the opposite direction, but the total spikes will be the same for the 2 directions. The solid lines show responses to the same 2 stimuli for an idealized cell that shows preferred-direction facilitation and null-direction suppression. The response in the preferred direction (1 then 2) is larger than the linear sum (facilitation), but the response in the other direction is smaller than the linear sum (suppression). The difference between the actual response and the linear sum is the interaction.

cd/m^2. For the black-and-white stimulus trains, when black and white stimuli overlapped they yielded background gray. In stimulus trains of pairs of light stimuli, gray stimuli were presented on a black background, and when two stimuli overlapped, the result was white. For stimulus trains of pairs of dark stimuli, the single stimuli were gray on a white background, and when two stimuli overlapped the result was black. For each map, between 5,000 and 50,000 spikes were collected over a 10- to 30-min period. Spikes were used for mapping only if the monkey's eyes were within the fixation window at the time of stimulus onset. Maps were smoothed with a Gaussian filter in both spatial dimensions; for cells with receptive-fields eccentricities less than 5° the sigma of the Gaussian was 0.15°; for cells with eccentricities greater than 10°, the sigma was 0.25°.

A computer recorded the spike train at 1-ms resolution and the eye position at 4-ms resolution. Spikes were reverse correlated with the relative positions (difference in position) of pairs of spots (Fig. 1, *C* and *D*). One spot was considered the *reference* stimulus, and the other, *probe* stimulus, was either the other stimulus in the same frame (for simultaneous interaction mapping) or in a preceding frame—the immediately preceding frame (13-ms intervals) or the frame preceding that (27-ms intervals), etc. Activity was mapped as a function of probe stimulus position minus reference stimulus position, in (2-D) visual space; the horizontal axis corresponds to the horizontal difference in position between the probe and the reference stimulus, and the vertical axis corresponds to the vertical separation. Thus the origin represents occasions when the two stimuli fell in exactly the same location; locations above the origin represent occasions when the probe stimulus was above the reference, etc. For sequential interaction maps, positions above the origin represent occasions when the probe stimulus was above the reference (a downward apparent-motion stimulus), and positions to the right of the origin represent occasions when the probe stimulus was to the right of the reference stimulus (a leftward apparent-motion sequence, etc. The reverse correlation delay (usually between 40 and 60 ms) used for the maps in this study corresponds to the time to peak response to the reference stimulus.

Interactions are mapped as a function of one stimulus position relative to another, and both the reference and the probe stimuli were presented throughout the stimulus range. Therefore the maps show the *average* paired-stimulus interactions across the receptive field (Fig. 1, *C* and *D*). Our justification for averaging interactions over all reference locations is that previous work has shown that in general complex-cell interaction patterns are independent of reference stimulus position (Gaska et al. 1994; Movshon et al. 1978a; Rybicki et al. 1972; Szulborski and Palmer 1990). Each stimulus in a frame is analyzed independently from the other; this is justified because the positions of the two stimuli are independent and random. We eliminate data collected when the monkey's gaze was not within 1° of the fixation spot because spikes occurring when the monkey was looking elsewhere would dilute the signal with noise.

To examine those parts of the response that depend on the relative positions and sequence of pairs of stimuli, we must eliminate those aspects of the response that do *not* (Fig. 1*F*). The major part of the response that must be eliminated is the response to each stimulus presented independently, and one way to eliminate this contribution to the paired-stimulus response is by subtracting the inverting-contrast maps from the same-contrast maps [(white-to-white plus black-to-black) minus (black-to-white plus white-to-black)]. This same-minus-inverting calculation was derived from Wiener-kernel analysis by Emerson et al. (1987) for one-dimensional (1-D) ternary white-noise stimuli. Subtracting the inverting-contrast responses from the same-contrast responses eliminates the contribution of the stimuli presented independently because the response to a white-to-white stimulus pair consists of the response to the first white stimulus alone, plus the response to the second white stimulus alone, plus the interaction between the two, and so on for each stimulus contrast pair. Subtracting the inverting-contrast sequences from the same-contrast sequences cancels out all the responses to each stimulus alone, leaving only that part of the response that depends on stimulus pairing, for all four possible pairwise combinations of stimulus contrast. Because our stimuli were not Gaussian in either luminance or stimulus position, they would not fit the criteria for true Wiener-kernel analysis.

Because stimuli were presented every 13 ms, 13 ms is the temporal resolution of our mapping. Maximum interaction strength using the same-minus-inverting calculation was observed at the reverse correlation delay corresponding to the peak response time of the reference stimulus, so this is the delay we used; the interactions were weaker 13 ms before or after that, and negligible at all other delays (see Fig. 2, *top*). Previous 2-D interaction studies either used an optimal time slice for the reverse correlation delay (Livingstone et al. 2001; Szulborski and Palmer 1990) or averaged interactions over delays of 0–200 ms (Gaska et al. 1994).

For most of the maps in this study, we show interactions between stimuli in sequential frames (13 ms apart). Interactions between stimuli separated by two frames were weaker, and interactions between stimuli at even longer intervals were weaker still, becoming undetectable for all cells by 133 ms (10 frames) (Fig. 2, *bottom*).

To look at interactions between specific contrast combinations or to look at interactions between simultaneously presented same-contrast stimuli, we developed a different calculation to eliminate the linear component of the responses—the "long-interval subtraction" method (Livingstone et al. 2001). In this method, we subtract the paired-stimulus map obtained using a long (250 ms) interstimulus interval from the map obtained using the desired interstimulus interval. We use 250 ms because we determined (using a same-minus-inverting calculation) that there were no interactions between stimuli at such a long interval (see Fig. 2, *bottom*). Thus the 250-ms interval map depends only on the sensitivity of the cell and the number of stimulus presentations at each spatial position, and therefore can serve as a linear map, which we can subtract from the map obtained at the desired interstimulus interval. This leaves only activity due to paired-stimulus interactions (2nd-order nonlinear interactions). With the long-interval subtraction method, we can see directly whether interactions for any stimulus pair are facilitatory (larger than the independent combination) or suppressive (smaller than the independent combination). In Wiener-kernel analysis, positive interactions are the sum of same-contrast facilitation and inverting-contrast suppression and negative interactions are the sum of same-contrast suppression and inverting-contrast facilitation. Thus from Wiener-kernel analysis you cannot tell if interactions are actually facilitatory or suppressive, whereas you can using the long-interval-subtraction method. We therefore refer to "positive" and "negative" interactions when we use same-minus-inverting calculations and to "facilitation" and "suppression" when we use the long-interval subtraction method.

Direction tuning curves were generated using fields of bars or fields or dots, as indicated, that moved across the receptive field for 0.5 s at each orientation; different directions were randomly interleaved. Numbers on each plot indicate the maximum average firing rate per sweep. Tuning bandwidth was measured as the angle subtended by the tuning curve at half-maximal response (Albright et al. 1984).

Subunit dimensions and amplitude

The elongation of the interaction regions of the same-minus-inverting sequential interaction map for each complex cell were determined in two ways. First, we generated contours at ±50% of the peak facilitatory magnitude and measured the maximum width along the direction axis and the maximum length along the orientation axis. As a second way of measuring the amplitude and dimensions of the facilitatory and suppressive regions, we fit them with a 2-D Gaussian function with seven free parameters. The fits were optimized via a least-squares criterion with the Levenberg-Marquardt algorithm in Matlab. The equation for the 2-D elliptical Gaussian function was

$$F(x, y) = A \exp(-p_x^2/2\sigma_x^2) \exp(-p_y^2/2\sigma_y^2) + \Omega$$

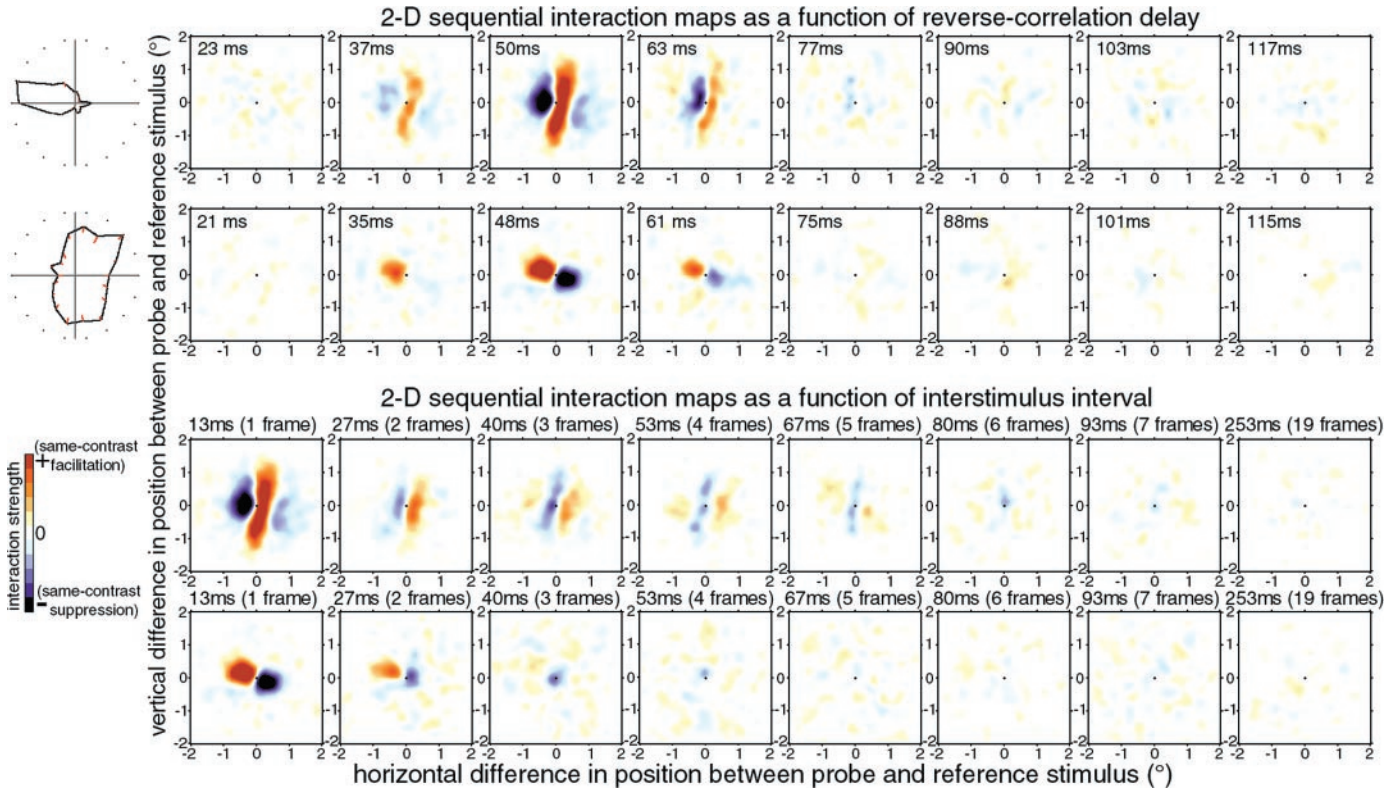

FIG. 2. Interaction maps for pairs of sequentially presented spots, for 2 complex cells as a function of reverse correlation delay (*top*) and inter-spot interval (*bottom*). Direction tuning curves (*left*) were generated using fields of moving bars. The 1st cell was recorded at an eccentricity of 22° and the 2nd at 21°. The 2-D interaction maps are the same-minus-inverting responses; red on the color scale indicates positive interactions (same-contrast facilitation and inverting-contrast suppression), and blue indicates negative interactions (same-contrast suppression and inverting-contrast facilitation). The reverse correlation delay indicated in the *top* is for the reference stimulus; the interstimulus interval was 13 ms (1 frame). For the bottom, the reverse correlation delay was 50 ms for the 1st cell and 48 ms for the 2nd.

where

$$p_x = (c_x - x)\cos\Theta + (c_y - y)\sin\Theta$$

$$p_y = (c_x - x)\sin\Theta + (c_y - y)\cos\Theta$$

A is the amplitude; c_x and c_y are the centers of the two Gaussians, σ_x and σ_y are the SDs of the Gaussians, Θ is the angle of the major axis, and Ω is the baseline offset.

The positive interaction region was thresholded at 20% of its peak height and then fit; the negative region was first inverted, thresholded at the same level, and then fit. The amplitude for each region was the amplitude of the best-fitting Gaussian. The length of each region was twice the σ corresponding to the orientation axis, and the width was twice the σ corresponding to the motion axis. This calculation gave the same relative lengths and widths as measuring contours at ±50% of peak.

Gradient of 2-D interaction maps

To correlate each cell's direction preference with the pattern of positive and negative interactions in the 2-D interaction maps, we calculated the slope (going from facilitatory to suppressive interactions) through the origin of the 2-D interaction maps. We calculated this by finding the local gradient through the origin of the 2-D interaction maps. To do this, we calculated the gradient for a distance corresponding to the average subunit width in both directions from the origin at every angle from 0 to 180° and calculated the vector average over all the angles.

Magnitude of paired-stimulus interactions

We measured the magnitude of the interactions by generating a square window that was placed just to the preferred-direction side (or the null-direction side) of the origin of a same-contrast sequential interaction map, centered on the maximum facilitatory (or the maximum suppressive) region. The window was as wide as half the average subunit width in the same-minus-inverting map. The number of spikes in the window for a 13-ms interstimulus interval was compared to the number of spikes in the window for a 250-ms interstimulus interval. The magnitude of the interaction, a percent difference, was taken as 100 times the number of spikes for the 13-ms interval minus the number for the 250-ms interval, divided by the number for the 250-ms interval. This measurement represents the average facilitation (or suppression) at the optimum interstimulus separation over the entire stimulus range, which includes regions outside the receptive field and thus must underestimate the maximum facilitation (or suppression) for pairs of stimuli localized to the receptive field.

Simple and complex cells

For all cells, 1-D space-time maps were generated using light and dark bars of the preferred orientation flashed at 75 Hz. For these maps, spike activity was mapped as a function of time after stimulus onset and stimulus position (corrected for eye position at the time of stimulus onset) (Livingstone 1998; Livingstone and Tsao 1999). Eye-position-corrected mapping was used in this study only to distinguish simple and complex cells and to generate the first-order maps in Figs.

4 and 5; the *interaction* maps use relative stimulus position, so eye position was not part of that calculation. Simple and complex cells were distinguished by measuring the phase difference between Gabor functions fit to spatial and temporal profiles of the light and dark-bar maps. Cells that showed a greater than 90° phase difference in temporal and spatial profiles for the white and black maps were considered as simple, and cells with smaller phase differences were considered to be complex (Conway and Livingstone 2002).

Model calculations

To generate the space-space-time energy model, in *x*, *y*, and *t*, shown in Fig. 9, the faster nondirectional component was calculated by multiplying a Gabor function in the *x* spatial dimension (the motion axis)

$$fx(x) = A \exp(-(x - c)^2/(2\sigma^2)) \cos(2\pi\upsilon(x - c) + \phi)$$

where A is the amplitude, c is the center, σ is the standard deviation of the Gaussian, υ is spatial frequency of the sinewave, ϕ is the phase of the sinewave; by three Gaussian functions with centers aligned along the *y* dimension (the orientation axis)

$$fy(y) = A \exp(-(y - c)^2/(2\sigma^2))$$

where A is the amplitude, c is the center, and σ is the standard deviation; and by a temporal function of the form

$$ft(t) = t^n e^{-t}\{1/n! - t^2/(n + 2)!\}$$

(Robson 1966), where $n = 15$.

The slower nondirectional component was generated by multiplying a Gabor in the *x* dimension, three Gaussian functions in the *y* dimension, and slower temporal function (same equation except $n = 17$), and the temporal function was rectified. For the energy model, the three Gaussians in the *y* dimension were summed before combining the two temporally different nondirectional units; for the localized-inhibition model, they were summed after combining the two temporally different nondirectional units.

Interactions between pairs of stimuli were calculated by rectifying then squaring (half-squaring) the sum of the responses to the two stimuli (the magnitude of the receptive-field map at that point), then subtracting the sum of the two responses, passed independently through the same half-squaring nonlinearity (Heeger 1992). For the energy model, interactions were calculated for pairs of points corresponding to the space/space maps of the oriented directional cell at the two times indicated.

For the localized inhibition model, there were three unoriented directional subunits, and interactions were calculated for all nine pairwise combinations, then summed. For each pairwise interaction, inhibition was not rectified before combining if the two responses were from the same subunit, but it was rectified before summing if the two were from different subunits. That is, all "two-stimulus responses" to pairs of stimuli were summed, rectified, then squared if they resulted from activation of the same unoriented unit, or they were rectified, summed, then squared if they resulted from activation of different unoriented units.

All procedures were approved by the Harvard Medical Area Standing Committee on Animals.

RESULTS

Second-order sequential interactions in directional cells; temporal properties

In the first series of experiments, we used a stimulus train in which the two stimuli in each frame were opposite in contrast—one black, one white (Fig. 1*B*). Figure 2 shows paired-stimulus interactions generated using a same-minus inverting calculation (see METHODS), for two complex directional cells, at various reverse-correlation delays and various interstimulus intervals. The interaction is maximum at a reverse correlation delay corresponding to the time to peak response (*top*) and strongest for interactions between stimuli occurring at 13-ms intervals (sequential frames; *bottom*). Therefore the maps shown in this study use these delays and intervals, unless indicated otherwise.

Both complex cells in Fig. 2 show localized regions of positive interactions (same-contrast facilitation) in map positions corresponding to preferred-direction sequences and negative interactions (same-contrast suppression) in map positions corresponding to null-direction sequences. Thus the pattern of nonlinear interactions is consistent with each cell's actual direction selectivity to moving bars. Both maps differ, however, in some ways from what was expected.

We will briefly consider here what we expect for the paired-stimulus interaction map for an ordinary oriented simple cell (and these nonlinearities will be preserved in complex cells receiving inputs from this cell), and we will model our predictions at the end of this paper. From previous work (Gaska et al. 1994; Sakai and Tanaka 2000; Szulborski and Palmer 1990) and from the hypothesis that complex cells are generated by combining simple cells (Hubel and Wiesel 1962), we would expect 2-D interaction maps of complex cells to show alternating elongated bands of suppressive and facilitatory interactions. Fig. 1*C* shows an idealized simple-cell receptive field, with an elongated ON region (light-excitatory/dark-inhibitory) and an elongated OFF region (dark-excitatory/light-inhibitory) to its right. If this is the organization of an input (or an input to an input) to a complex cell and if there is some static nonlinearity in the output of either this cell or the complex cell, the organization of this simple cell should be apparent in the paired-stimulus interactions of the complex cell (Sakai and Tanaka 2000; Szulborski and Palmer 1990). For simultaneously presented stimuli, the organization of this simple cell will be apparent as interactions between different parts of its receptive field. We will assume that pairs of stimuli presented in close temporal proximity will show nonlinear interactions, such as a half-squaring nonlinearity. (If there are no nonlinearities, there will be no interactions.) If two stimuli are both excitatory, we will assume that the combined response will be larger than the sum of the responses to the two stimuli presented independently; i.e. the interaction will be facilitatory. If one response is excitatory and the other inhibitory, the combined response will be smaller than the sum of the two responses to the stimuli presented independently; i.e. the interaction will be suppressive.

For each of the six positions labeled in this cell's receptive field (a–f), there will be six possible interactions for a total of 36 possible interaction pairs (for order-specific interactions, such as sequential interactions; Fig. 1*D*). The interaction of each position with itself will show facilitatory interactions for same-contrast stimulus pairs and will map to the origin of the interaction map as indicated. Other pairwise interactions will be facilitatory for same-contrast stimulus pairs in the same ON or OFF subregion and suppressive for same-contrast stimulus pairs in different polarity subregions. Thus a nonlinearity arising in a simple cell with only two subunits should consist of an elongated band of positive interactions (same-contrast facilitation, inverting-contrast suppression) flanked by two elongated bands of negative interactions (same-contrast suppression, in-

verting-contrast facilitation). Because each point can interact with parts of the receptive field above and below itself, the interactions should be even more elongated than the receptive field itself.

For sequential interactions, this cell should show interactions between each part of its receptive field at one point in time with each part of its receptive field at a subsequent point in time. The easiest model to consider is the energy model in which the organization of a simple-cell receptive field remains constant over time but shifts position spatially (Adelson and Bergen 1985). In this case, we would expect the same pattern of interactions for sequential stimuli just shifted with respect to the origin of the interaction map.

Now let us compare the predicted interactions with those we measured. The interaction map for the second cell in Fig. 2 is not elongated at all, and it shows only two round interaction regions, one positive and the other negative, quite unlike our prediction. The map for the first cell is more consistent with what we expect for an ordinary two-subunit simple cell because it has an elongated positive interaction region, flanked by two negative interaction regions; but the negative interaction regions are not as elongated as the facilitatory region. This interaction map indicates that sequential spots separated by a small fraction of the receptive field length along the orientation axis can show both facilitatory and suppressive interactions (depending on their relative positions along the direction axis), but spots separated by a longer distance along the orientation axis show predominantly facilitatory interactions. Thus the standard energy model of complex directional cells built from space-time offset simple cells will not completely explain either type of map.

Kinds of sequential interaction maps

Figure 3 shows two-spot sequential interaction maps for 12 complex direction-selective cells from macaque V1. These cells are qualitatively similar to our entire population of complex cells, although they were chosen for illustration because they had the largest magnitude interactions and therefore the clearest maps. For each cell, the direction tuning to bars and the receptive-field eccentricity are shown to the left of the interaction map. For each cell, the interaction map shows positive interactions for preferred-direction sequences and negative interactions for null-direction sequences. The interactions of the cells on the left, like the second cell in Fig. 2, showed robust directional interactions, but the interactions were not elongated at all along the orientation axis and they consisted of only two regions, one positive and the other negative. The interaction maps on the *right*, however, were elongated along the orientation axis, and some had more than just two regions, as predicted. However, the negative interactions were more localized along the orientation axis than were the positive interactions, resulting in a subtle inflection at the origin and an overall chevron shape (Fig. 3, *right*). The ends of the chevrons always bent toward the null side of the receptive field. [We will refer to the side from which null-direction stimuli arise as the "null side" after He and Masland (1997)]. Similar inflections, or crescent-shaped interaction maps, were previously observed using exactly the same mapping technique in macaque MT (Livingstone et al. 2001).

Thus although the paired-spot sequential interaction maps were consistent with the idea that complex cells are made up from repeating subunits, none of the maps were exactly what would be predicted if those subunits were ordinary oriented simple cells—the interaction maps with pairs of round interaction regions were too short along the orientation axis, and the elongated maps were not homogeneous along the orientation axis. The simplest explanation for the round interaction maps is that the subunits are not elongated perpendicular to the direction axis; that is, that they are center-surround rather than orientation selective, like geniculate or layer 4C cells. The chevron-shaped maps seem more difficult to explain.

Interaction maps for simple cells

We then asked whether the shape of the complex-cell interactions might arise from the interaction patterns of antecedent simple cells. We obtained the clearest interaction maps from complex cells, but we did get fairly clear interaction maps for some simple cells, and both first- and second-order maps are shown for seven simple cells in Fig. 4. Surprisingly, at least some of the simple cells did not have elongated ON and OFF subregions in their first-order, receptive-field maps as originally observed by Hubel and Wiesel (1962) but rather had one round ON subregion adjacent to a round OFF subregion. Only a few of the simple cells, like the next-to-last one in Fig. 4, had clearly elongated ON and OFF subregions. Thus the round-interaction complex cells could be explained by having inputs from simple cells with round subunits. Unfortunately the simple-cell interaction maps were not clear enough or abundant enough for us to conclude whether more elongated simple cells typically show chevron-shaped interactions or the predicted band-like interactions. As we discuss later, the existence of round-interaction directional cells might explain the chevron-shaped interactions in the elongated cells.

Interaction maps for fixed reference positions

The second possibility we examined to explain the odd chevron shape is that it represents a summation of interactions that are oriented differently for different parts of the receptive field. So we looked at subsets of the interactions selected from the same spike train, restricted to occasions when the reference location was constrained to be within one part or another of the receptive field. This analysis is shown for four complex cells in Fig. 5. All the analyses for each cell were from a single stimulus run using one black spot and one white spot per frame. For each cell a first-order (receptive-field) map was calculated for white and black stimuli, and the receptive field was divided into thirds along the orientation axis as indicated (Fig. 5, purple boxes). Paired-stimulus sequential interaction maps were calculated using same-minus-inverting responses for reference locations lying anywhere in the stimulus range or within each third of the receptive field as indicated. In general, for cells with round interactions, the maps were identical for reference positions localized to each part of the receptive field (*bottom row*). For cells with elongated, chevron-shaped interactions, the maps from each part of the receptive field were elongated, with the facilitatory interactions in particular elongated asymmetrically for reference locations at one end or the other of the orientation axis. That is, looking at the *top row* of

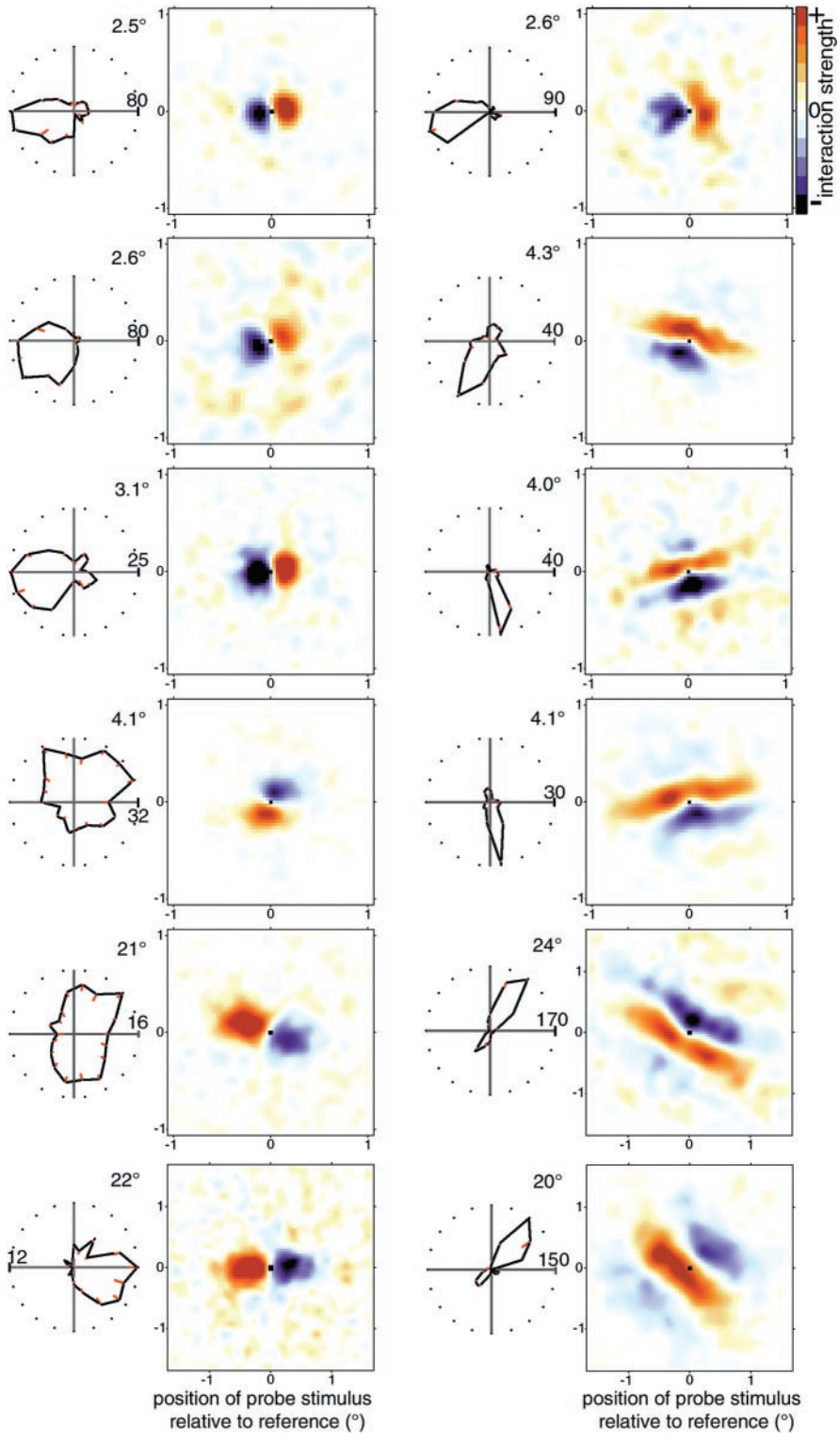

FIG. 3. Direction tuning curves and 2-D sequential 2-spot interaction maps for 12 complex cells recorded in macaque V1. Direction tuning curves were generated using fields of moving bars; the number on the tuning curve indicates the maximum average firing rate per sweep in spikes/s; error bars (red) indicate SE. Receptive-field eccentricity of each unit is indicated *above* and to the *right* of each tuning curve. All the units were recorded during different recording sessions, except the 4th unit down in both columns, and these 2 units were recorded simultaneously from the same electrode as 2 clearly distinguishable spikes with almost opposite direction preferences. The 2-D interaction maps are plotted according to the same conventions as Fig. 2. The pairs of stimuli were from sequential frames (13-ms intervals).

Fig. 5, facilitatory interactions for reference locations at the top of the receptive field extended more downward than upward, and facilitatory interactions with the bottom of the receptive field extended more upward. As discussed in the preceding text, the extension of the positive interactions along the orientation axis toward the other end of the receptive field is exactly what we would expect for a cell with simple-cell substructure, but the shorter negative interactions are not.

We can see in Fig. 5 that for complex cells the optimum interaction distance (the distance from the origin to the peak facilitatory or peak suppressive interaction) is small compared to the dimensions of the activating region. This indicates a subunit structure within the cells' receptive fields; this is what we would expect if each complex cell received input from several antecedent simple cells. In comparison, Fig. 4 shows that for simple cells the optimum interaction distance in the

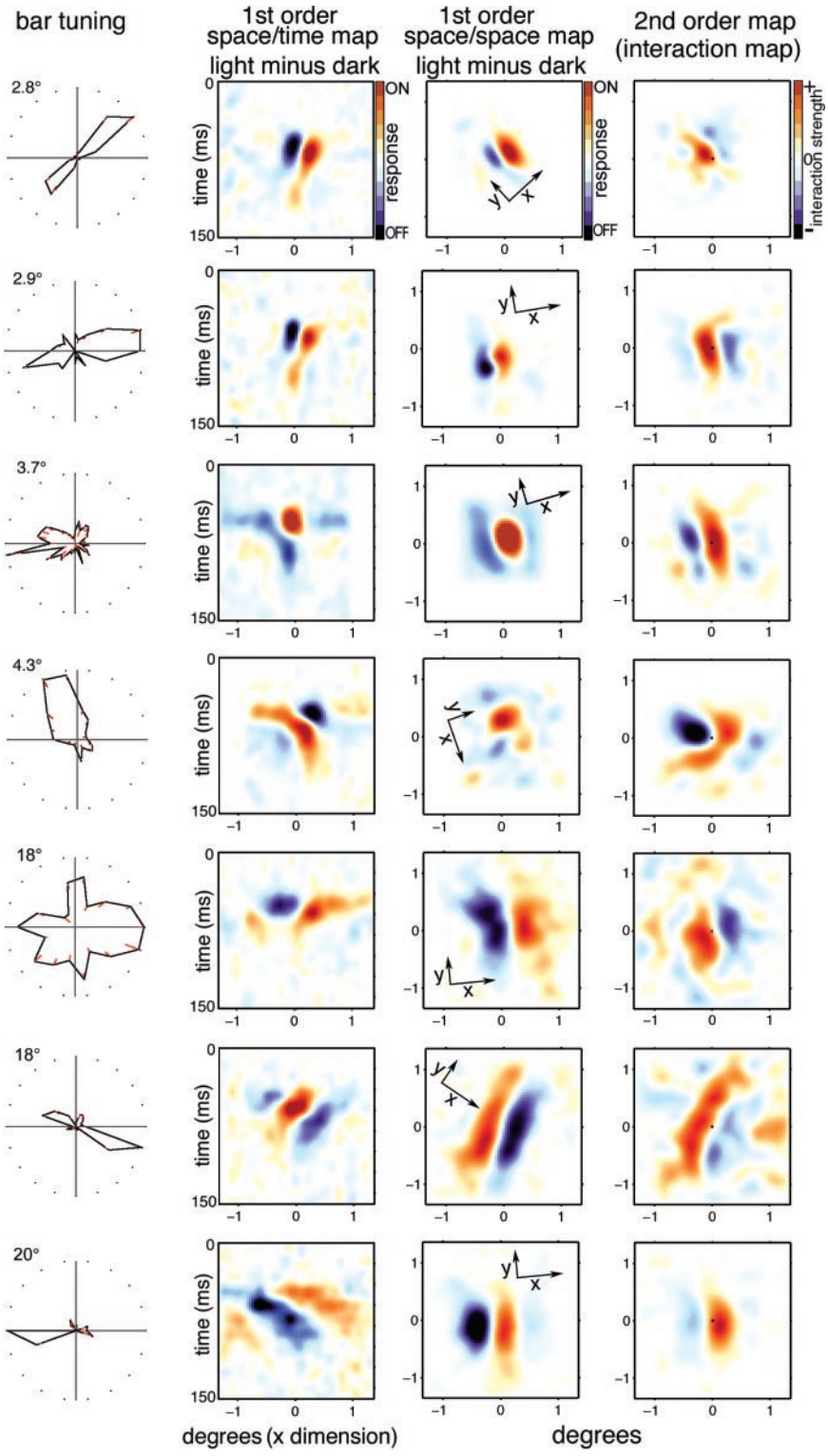

FIG. 4. Direction tuning curves, 1-dimensional (1-D) space/time maps, 2-D receptive-field maps, and 2-D sequential 2-spot interaction maps for 7 simple cells recorded in macaque V1. Each row shows data for one cell. *Left*: direction tuning curves were generated using fields of moving bars; error bars (red) indicate SE. Receptive-field eccentricity of each unit is indicated above and to the left of each tuning curve. *Left middle*: 1-D space-time maps were calculated by reverse correlating activity with eye-position-corrected bar location along a 1-D stimulus range (Livingstone 1998); color scale reflects spike activity, light minus dark. The spatial dimension is the direction axis, perpendicular to the preferred orientation—this is the axis indicated as *x* in *right middle. Right middle*: 2-D receptive fields were calculated by reverse correlating activity with eye-position-corrected spot location (Livingstone 1998); color scale reflects spike activity, light minus dark. Orientation (*y*) and direction (*x*) axes are indicated. *Right*: sequential interaction maps were calculated using same-minus-inverting responses; scale reflects interaction strength. The pairs of stimuli were from sequential frames (13-ms intervals).

interaction maps is comparable to the subunit spacing in the first order (receptive-field) maps.

Quantitative analyses

Figure 6 shows some quantitative analyses of the interaction maps. *A* shows the correspondence between the gradient of the complex-cell same-minus-inverting interaction maps versus the preferred direction of motion for fields of bars ($n = 63$). The gradient of the 2-D interaction maps gives the direction of maximum slope through the origin (from positive interactions to negative). The correspondence between the gradient of the 2-D interaction maps and the actual preferred direction of motion (measured with moving bars) is excellent, and supports the idea that the interaction maps reflect the mechanisms underlying direction selectivity (Gaska et al. 1994).

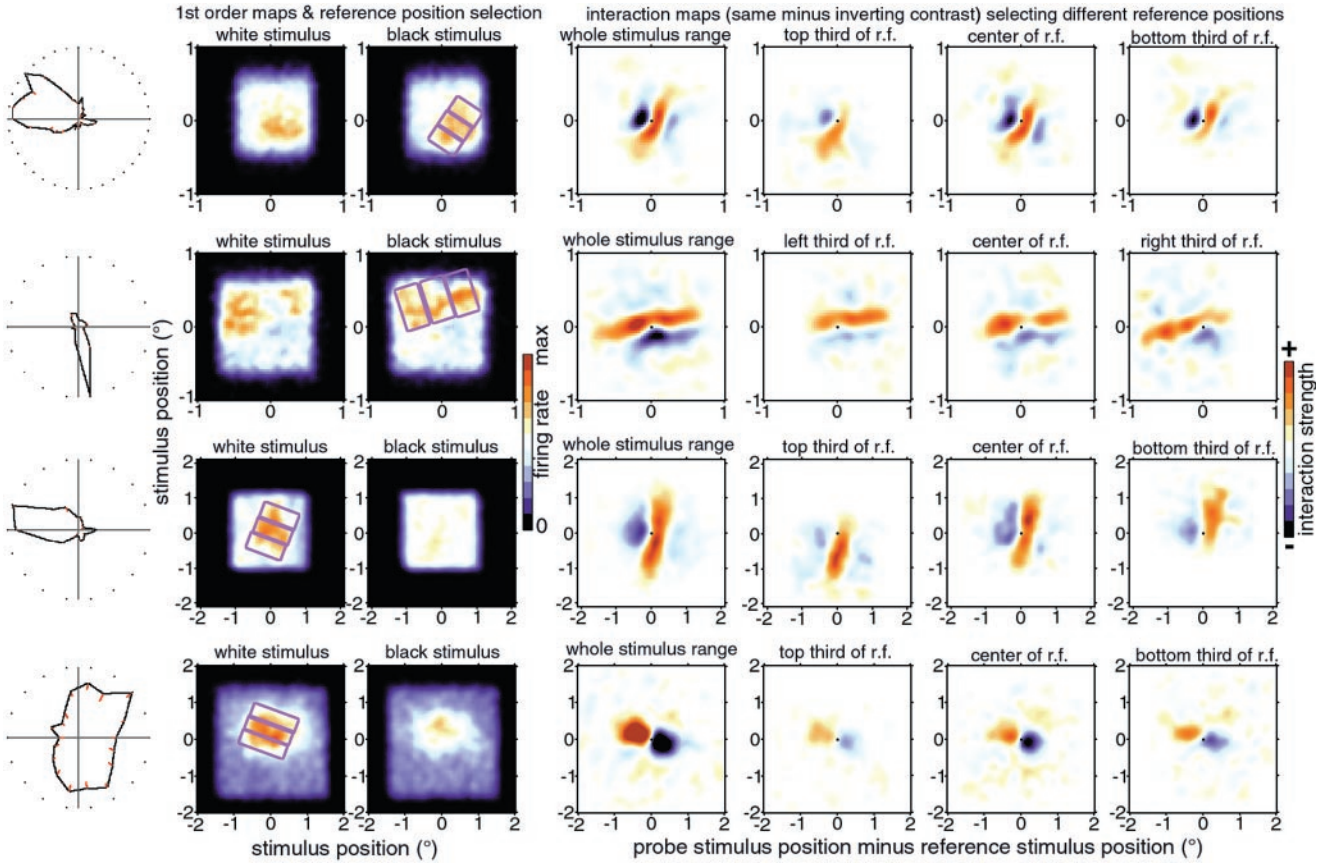

FIG. 5. 2-D sequential interaction maps using a small range of reference locations. Each row shows data from 1 cell. *Left*: the direction tuning to fields of bars. *2nd* and *3rd columns*: 1st-order (receptive-field) maps of responses to light and dark small spots at a reverse correlation delay corresponding to time to peak response. These were complex cells, so there is no obvious substructure to the receptive-field maps. The rectangles drawn on the receptive field indicate the regions selected for the reference stimulus location. *Right 4 columns*: paired-spot interaction maps for sequential stimuli (13-ms intervals); same-minus-inverting maps. *Third column*: maps for the entire stimulus range; *4th–6th columns*: the interaction maps generated from the same stimulus train using reference stimuli restricted to 1 of the 3 regions indicated on the 1st-order map.

Simple cells showed 2-D interactions that were qualitatively similar to the complex-cell interaction maps, except they were weaker (Figs. 3 and 4). We compared the magnitudes of the nonlinearities for simple and complex cells for sequential interactions at 13-ms intervals for all the cells in our population in Fig. 6*B*. The magnitude of the interaction was measured as the difference between the paired-stimulus response and the response to the two stimuli presented independently (at long interstimulus delays) as a percentage of the response to the two stimuli presented independently (see METHODS). Note that this magnitude measurement represents the average percent facilitation (or suppression) of the response to a pair of small flashed spots depending on whether the spots were flashed in a preferred (or null) apparent motion sequence compared to when they were flashed independently. This average magnitude must be smaller than the maximum facilitation (or suppression) because the interactions were averaged over the entire stimulus range not just the center of the receptive field. For each cell, the magnitude of the interactions on the preferred-direction side of the origin in the interaction maps, that is, interactions between stimuli presented at 13-ms intervals in the preferred direction, are plotted along the horizontal axis. The magnitudes of the null-direction interactions are plotted along the vertical axis. For all but one of the simple cells (●) and all the complex cells (□), the preferred-direction interactions were always facilitatory. On average the preferred-direction facilitation was larger for the complex cells (average = 54% facilitation) than for the simple cells (average = 28% facilitation). For null-direction sequences (vertical axis, Fig. 6*B*), most of the interactions were suppressive, although a few simple cells showed slightly facilitatory interactions in the null direction. Again, the suppression was on average larger for the complex cells (average = 29% suppression) than for the simple cells (average = 12% suppression). Jacobson et al. (1993) also found, in anesthetized macaque, that both simple and complex cells show nonlinear interactions and that the interactions are larger for complex cells than for simple cells. This larger nonlinearity of the complex cells might reflect either a nonlinearity at the complex-cell stage, in addition to the input simple-cell nonlinearity, or the cumulative nonlinearities of many input simple cells.

We asked whether it is generally true that cells with elongated interaction maps had narrower direction tuning curves than the cells with less-elongated interaction maps as suggested in Fig. 3. To address this question, we measured the length-to-width ratio of the positive and the negative interaction regions in the same-minus-inverting interaction maps (see METHODS). The average length to width ratio for the positive and negative regions for each of the directional complex cells

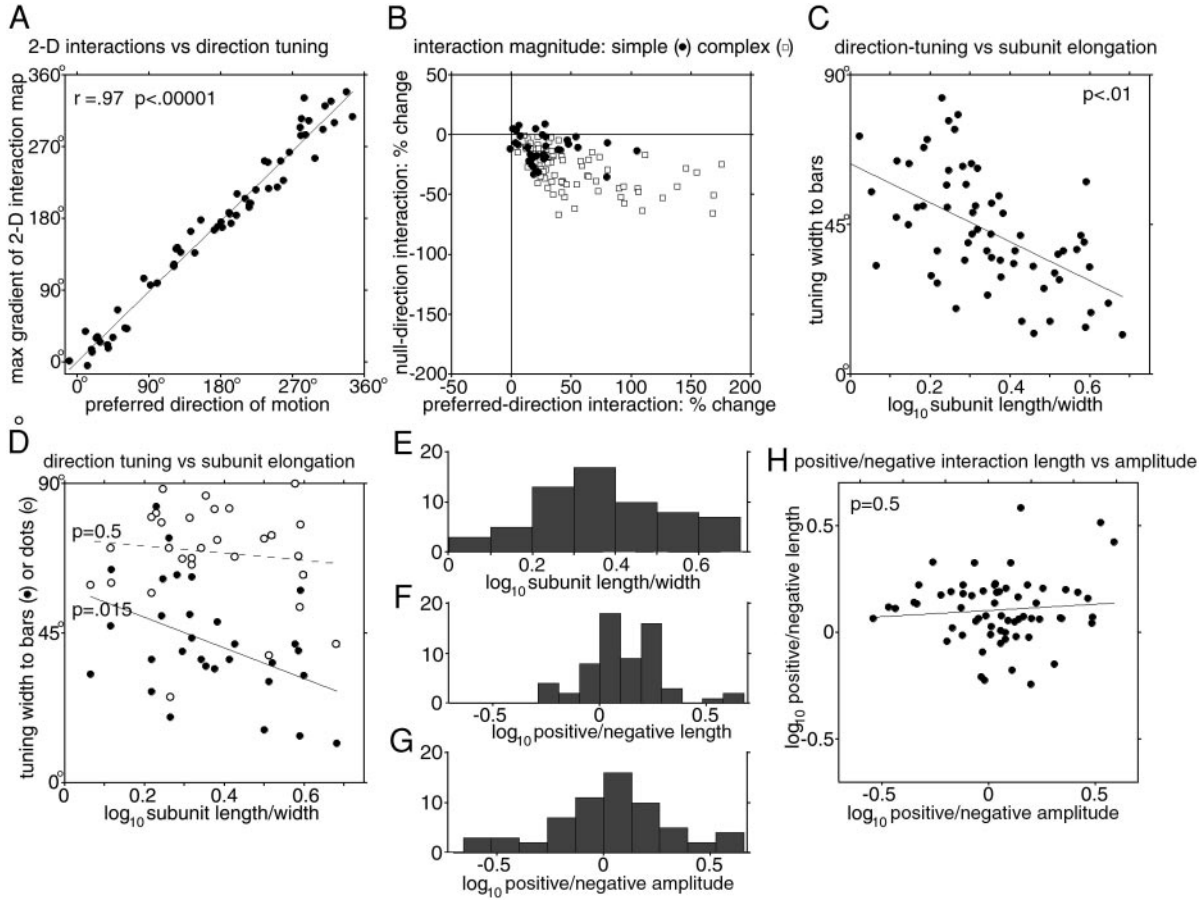

FIG. 6. Quantification of 2-D interaction maps. *A*: direction of the maximum gradient (from positive to negative interactions) of the 2-D sequential interaction map (same-minus-inverting) plotted against the actual preferred direction to moving bars. *B*: the magnitude of the nonlinearities for null and preferred sequences for simple (●) and complex cells (□). Nonlinearities for null-direction sequences are plotted on the vertical axis and nonlinearities for preferred-direction sequences on the horizontal axis. Interactions (the difference between sequential responses and responses to the same stimulus pairs at long interstimulus intervals) were measured for sequential same-contrast stimuli (for whichever contrast gave the larger interaction) as a percentage of the responses to the same two stimuli presented independently (250 ms apart). Complex cells on average showed larger nonlinearities than did simple cells. *C*: elongation ratio (width of direction kernel subunit/length) vs. direction tuning bandwidth to fields of bars. Cells with elongated interaction maps tended to have narrower direction tuning curves. *D*: elongation ratio vs. direction tuning bandwidth to fields of bars (●) or fields of dots (○). Cells with elongated interaction maps tended to have narrower tuning to bars but not to dots. *E*: histogram of the distribution of average interaction subunit elongation. Round interaction maps would have a low length/width ratio, and elongated maps would have a high ratio. *F*: histogram of the ratio of the lengths of positive and negative interaction regions for each cell. The distribution is significantly larger than a ratio of 1 (log = 0). *G*: histogram of the ratio of the amplitudes of positive and negative interaction regions for each cell. This distribution is not significantly different from a ratio of 1. *H*: the ratio of the positive interaction region length to the negative interaction length vs. their relative amplitudes. This shows that the fact that most positive interaction regions were longer than the negative interaction regions (*F*) cannot be explained by an amplitude difference.

for which we had same-minus-inverting maps ($n = 63$) is plotted in Fig. 6*C* as a function of the width of the direction tuning curve (to fields of bars) at half maximum response. The negative correlation between the tuning width and the subunit elongation is significant at the $P < 0.01$ level. Thus cells with elongated sequential interaction maps did tend to have narrower tuning curves.

Because the stimulus for the tuning curves in Figs. 3 and 6*C* was a field of bars, the narrowness of the tuning curves could reflect either orientation selectivity to the bars or the degree of direction tuning. Once it became clear to us that the narrowness of the tuning, and not just the direction preference, might be correlated with our interaction maps, we began using both bars and dots to measure direction tuning. So for a subset of the cells ($n = 30$), we can compare the subunit elongation to the direction tuning to fields of dots and to fields of bars (Fig. 6*D*). For this smaller population, the *bar* direction tuning width was still negatively correlated with the subunit elongation, but the direction tuning width to *dots* was not. Therefore it appears that the narrow tuning of cells with elongated interaction regions reflects narrow orientation tuning rather than narrow direction tuning.

Although we showed examples of round interaction maps and examples of elongated interaction maps in Fig. 3, the distribution of interaction region elongation did not appear to be bimodal (Fig. 6*E*). Thus the cells whose interactions are mapped in Fig. 3, *left* and *right*, likely represent the extremes of a continuum.

It was our impression that many cells' sequential interaction maps were chevron-shaped with the concavity toward the null side of the receptive field (Fig. 3, *right*) and that few if any

cells' interaction maps were bent in the opposite direction. We suspect that this chevron shape is secondary to a difference in elongation between positive and negative interactions: because negative and positive interactions cancel each other, if the negative interactions are shorter than the positive interactions, the ends of the positive interactions will not be cancelled as much as the middle, making the positive interactions appear "bent." Figure 6*F* shows the distribution of the ratio between the lengths of the positive and negative interaction regions; the geometric mean of the ratios was 1.3. A two-tailed *t*-test showed that we can reject the hypothesis that the lengths are the same (the log is 0) at the $P < 0.001$ level.

One might think that a systematic difference between positive interaction and negative interaction lengths could be explained by a difference in magnitude between facilitatory and suppressive interactions (or excitatory and inhibitory inputs). And indeed on average, the preferred-direction *facilitatory* interactions for the optimum contrast were larger in magnitude than the null-direction *suppressive* interactions (Fig. 6*B*). However, the single-contrast facilitation versus suppression comparison in Fig. 6*B* shows only part of the contribution to the same-minus inverting maps. In the same-minus-inverting maps, the interactions are the sum of the same-contrast interactions (white-to-white and black-to-black) minus the inverting-contrast interactions (white-to-black and black-to-white), while the interactions mapped in Fig. 6*B* represent only a single same-contrast interaction (white-to-white or black-to-black, whichever was larger). As shown in Fig. 6*G*, when we compared total positive to total negative interactions, there was not a preponderance of positive over negative interaction *magnitude* (geometric mean of positive to negative amplitude = 1.1); two-tailed *t*-test cannot reject the hypothesis that the amplitudes are the same at the $P < 0.05$ level.

Altogether, 49 of the complex directional cells had a positive interaction region that was longer (along the orientation axis) than the length of the negative interaction region; only 13 cells showed the reverse, consistent with our impression that most of the elongated interaction maps were bent with the concave side toward the null side of the receptive field and seldom the reverse. Figure 6*H* shows the lack of correlation between the ratio of the lengths of the positive and negative interaction regions and their amplitudes. So it cannot be the case that the difference in length of the positive and negative interactions is due to a difference in magnitude. There was also no correlation between tuning width to bars and the positive to negative interaction magnitude (not shown).

From the quantitative comparisons in Fig. 6, we conclude the following. *1*) The patterns of facilitatory and suppressive interactions are tightly correlated with direction selectivity. *2*) Both simple cells and complex cells show preferred-direction facilitation and null-direction suppression; complex cells show interactions that are on average larger than the interactions for simple cells, and facilitatory interactions, for same-contrast stimuli are on average larger than suppressive interactions. *3*) Cells with round interactions are broadly tuned for orientation, and cells with elongated interactions are more narrowly tuned for orientation. *4*) Positive interactions extend farther along the orientation axis than negative interactions, and this cannot be explained by a simple difference in magnitude between positive and negative interactions. We postulate that this difference in elongation results in a slight apparent bend in the interaction maps with the concave side toward the null side of the receptive field.

Long-interval-subtraction—an alternative to Wiener-like kernel analysis

To see directly how the shape of the facilitatory interactions compares to the shape of the suppressive interactions and to see directly how inverting-contrast interactions compare to same-contrast interactions, we used a long-interval subtraction method (see METHODS), which does not require combining responses to all four contrast-pairs as the same-minus-inverting calculation does. In this calculation, we subtract the paired-stimulus map at a long interstimulus interval (we established that there were no interactions between pairs of stimuli at this long interval—Fig. 2) from the map at the desired interstimulus interval. This subtraction leaves only the activity due to paired-stimulus interactions. Because the same-minus-inverting calculation sums same-contrast facilitation with inverting-contrast suppression and vice versa, it cannot distinguish facilitation from suppression. The long-interval subtraction method, however, shows directly whether the average response to a particular pair of stimuli is larger or smaller than the combined responses to the same two stimuli presented independently.

Figure 7 shows sequential interaction maps for each contrast pair individually (from the black-and-white stimulus train) for a complex cell that preferred motion down and slightly to the right; this is the same cell as in Fig. 3, *right, 3rd panel* from the *top.* Because this is a downward-preferring cell, the null-direction interactions lie below the origin and preferred-direction interactions lie above the origin. For same-contrast pairs of sequential stimuli (white-to-white and black-to-black), the interaction maps show facilitation when the preceding stimulus was above the reference stimulus (i.e. the apparent-motion sequence was downward, the cell's preferred direction) and suppression when the preceding stimulus was below the reference stimulus (i.e. the sequence was upward, the cell's null direction). The reverse is true when the two stimuli were of opposite contrast (black-to-white and white-to-black). In other

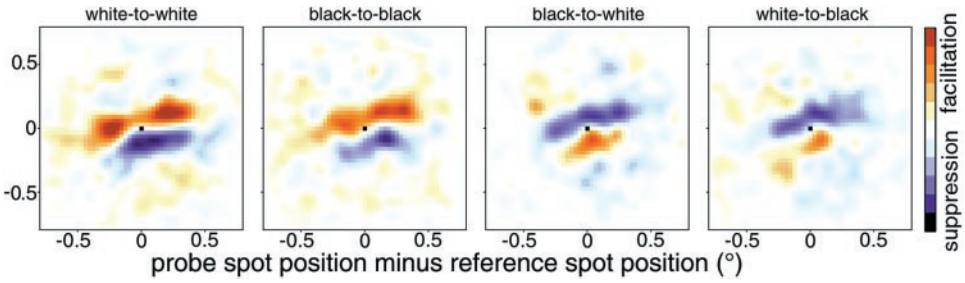

FIG. 7. Sequential interaction maps for all contrast combinations for 1 complex cell calculated using the long-interval-subtraction method (see METHODS); all maps were calculated from the same spike train. Color scale reflects facilitatory and suppressive interactions. This is the same cell as in Fig. 3, *right, 3rd* from the *top*. Note the reversal of the interaction pattern for inverting-contrast stimulus pairs.

words, for same-contrast sequences, responses were larger in the preferred direction than in the null direction, consistent with the cells' tuning to moving bars, but for inverting sequences, responses were larger in the null direction than in the preferred direction. This means that this cell's 2-D sequential interactions show reverse phi—a perceptual phenomenon in which an apparent-motion sequence is perceived as moving the opposite direction than it actually does, when the stimuli invert contrast (Anstis and Rogers 1975). In all four maps, the preferred-direction interaction regions are longer than the null-direction interaction regions: for the same-contrast maps, the length of the preferred-direction facilitation is 1.4 (white-to-white) and 1.5 (black-to-black) times the length of the null-direction suppression; for the inverting-contrast maps, the length of the preferred-direction suppression is 1.8 (black-to-white) and 1.6 (white-to-black) times the length of the null-direction facilitation. The inverting-contrast interactions are just about the inverse of the same-contrast interactions, indicating almost complete contrast-opponency in the mechanisms generating the nonlinearities in this cell's responses, despite the fact that this was a complex cell and did not show contrast opponency in its receptive-field map.

Simultaneous versus sequential interactions—orientation versus direction

Sequential interaction maps confound directional and orientation interactions, but orientation interactions can be isolated by looking at interactions between simultaneously presented stimuli. To map both simultaneous and sequential interactions from the same stimulus train, we used stimulus trains in which two stimuli of the same contrast were presented in each frame. The stimulus configuration was identical to that illustrated in Fig. 1, except each frame consisted of two stimuli of the same contrast; in any stimulus run, the stimuli were all white or all black. Again we used the long-interval-subtraction method to calculate interactions between simultaneous (interval = 0 ms) or sequential (interval = 13 or 27 ms) stimulus pairs.

Each row in Fig. 8 shows simultaneous and sequential interaction maps generated using two white squares per frame (odd rows) or two black squares per frame (even rows) for three complex directional cells. The sequential interaction maps for 13-ms intervals are similar in shape to the interaction maps for the same cells generated using the black-and-white stimulus sequence and same-minus-inverting calculation.

The most dramatic change in the structure of the interactions between the simultaneous and sequential pairs (compare Fig. 8, *B* with *C*) is that the simultaneous pairs produce interactions that are symmetric about the orientation axis, with a blob of blue suppression on each side of the red barbell of facilitation, and the sequential interactions are asymmetric about the axis of orientation, with the suppressive blob on the preferred side disappearing. This is also shown in the maps of the contours (*E*). Note that the facilitatory interactions and the suppressive interactions also shift slightly in the preferred direction as predicted by Sakai and Tanaka (2000).

Models

It has been proposed (Adelson and Bergen 1985) that directional simple cells are generated by combining nondirectional simple cells that have different temporal properties. It is sometimes assumed that these nondirectional inputs are themselves orientation-selective simple cells. Here we explore the possibility that directional interactions precede, rather than follow, elongation of the receptive along the orientation axis. Some directional cells show elongated directional interactions and others do not (Fig. 3). Moreover, in those cells with elongated interactions, negative interactions are usually less elongated along the orientation axis than are positive interactions. And the ends of the positive-interaction regions show less directional shift with interstimulus interval, compared with the center interactions. This is consistent with the possibility that some directional interactions occur before or at the stage of receptive-field elongation along the orientation axis. Both the round interaction maps and the elongated interaction maps suggest this—the round-interaction maps because they show directional interactions but no elongated interactions and the elongated maps because the directional interactions are less elongated along the orientation axis than the orientation interactions.

The interactions mapped in a complex cell presumably reflect the cumulative interactions from the same and antecedent stages (Gaska et al. 1994; Szulborski and Palmer 1990). Sakai and Tanaka (2000) modeled the expected interactions for a complex cell made up either from simple cells or simple-cell-like dendritic compartments and found that the interaction maps for a complex cell made up from oriented simple cells should show elongated bands of positive and negative interactions as found by Szulborski and Palmer (1990) and that the shapes of the maps were invariant with phase and position of the simple-cell receptive fields.

We will consider interactions arising from a conventional, push/pull simple cell, with ON subregions that are light-excitatory/dark-inhibitory and OFF subregions that are dark-excitatory/light-inhibitory. To model interactions, we assume that each point in the stimulus range, or in the receptive field, can serve as a reference location and as a probe location. For a static nonlinearity, such as half squaring (Heeger 1992), when the probe and the reference stimuli are of the same contrast, interactions will be facilitatory if the two stimuli are presented simultaneously within subregions of the same polarity (both ON or both OFF), but they will be suppressive if they are presented within subregions of opposite polarity (one ON, the other OFF). If the two stimuli are of opposite contrast, interactions will be suppressive when presented within same-polarity subregions and facilitatory when presented in opposite-polarity subregions.

In Fig. 9, we model the expected 2-D interaction maps for directional cells in which orientation is generated before direction selectivity and the reverse. Here we must distinguish between receptive-field elongation and orientation selectivity. As Hubel and Wiesel (1962) originally pointed out, orientation selectivity could be produced by displacement of excitatory inputs along the axis of orientation (elongation of the receptive field) or by the separation of excitatory and inhibitory subregions along the perpendicular axis. There is experimental support for both mechanisms. In *A*, we assume that receptive-field elongation occurs before direction selectivity, as proposed in Hubel and Wiesel (1962); in *B*, we assume that receptive-field elongation occurs after the generation of direction selectivity.

For both models in Fig. 9, we generated a space-time-slanted

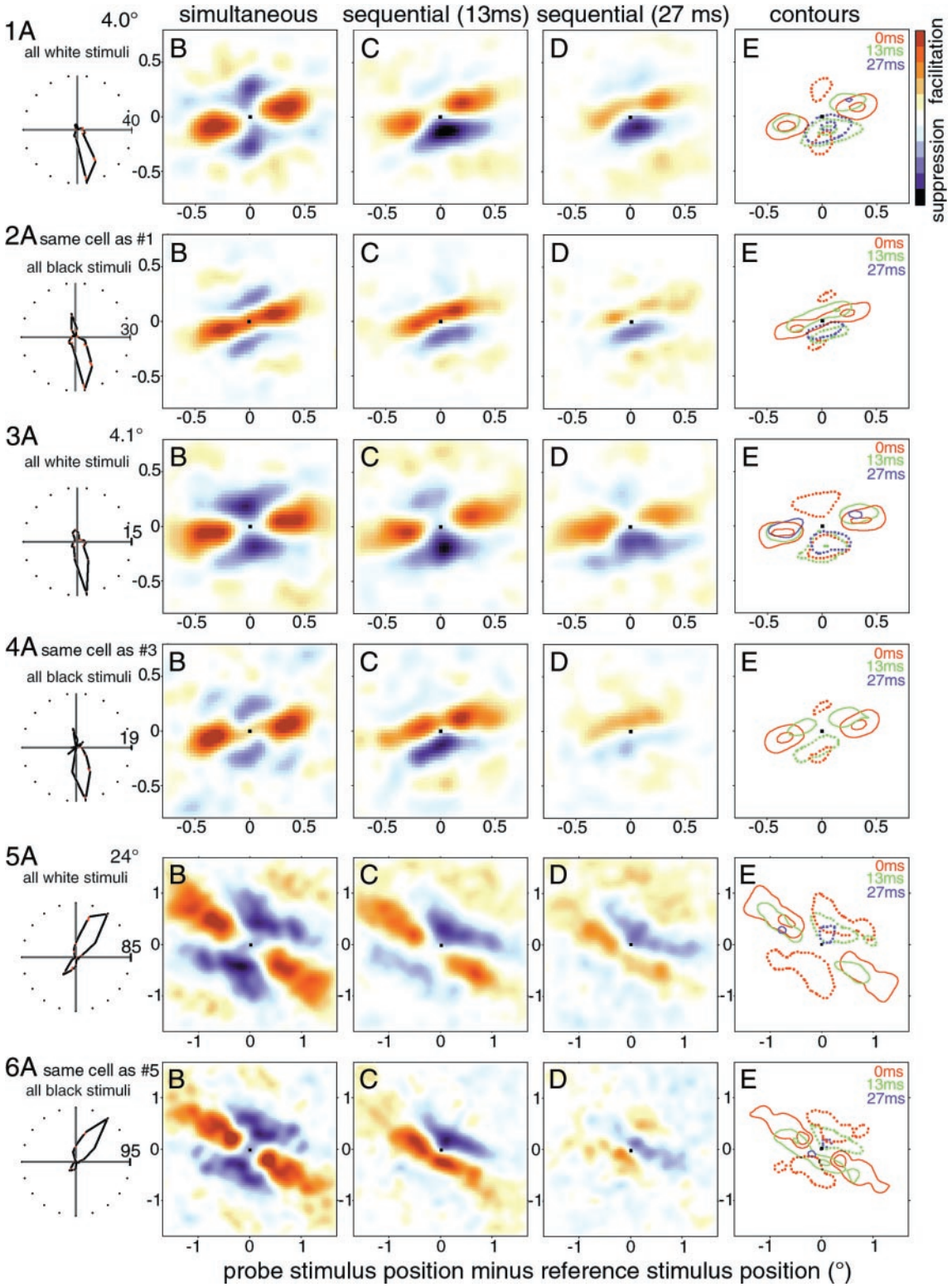

FIG. 8. Simultaneous and sequential interaction maps for 3 complex cells calculated using the long-interval-subtraction method. Each pair of rows is from a single cell (1 and 2, 3 and 4, 5 and 6). For comparison with the same-minus-inverting interaction maps, these 3 cells are, in order, the same cells as the 3rd, 4th, and 5th cells from the *top* on the *right side* of Fig. 3. *A*: direction tuning for white or black bars. *B–D*: 2-D 2-stimulus interaction maps for pairs of white stimuli (odd rows) or pairs of dark stimuli (even rows) at interstimulus intervals as indicated at the top of each column. All maps in each row were calculated from the same spike train. *E*: contour plots of the maps in *B–D* showing the shift in interactions with different interstimulus intervals; —, facilitatory interactions; · · ·, suppressive interactions.

direction-selective cell by summing the inputs from non-space-time-slanted (separable) nondirectional cells, as proposed in the original energy model (Adelson and Bergen 1985), with a minor modification: we model the slower component as temporally monophasic because principal component analyses of direction-selective simple cells suggest this is the case (De Valois et al. 2000; Kontsevich 1995; Conway and Livingstone 2003).

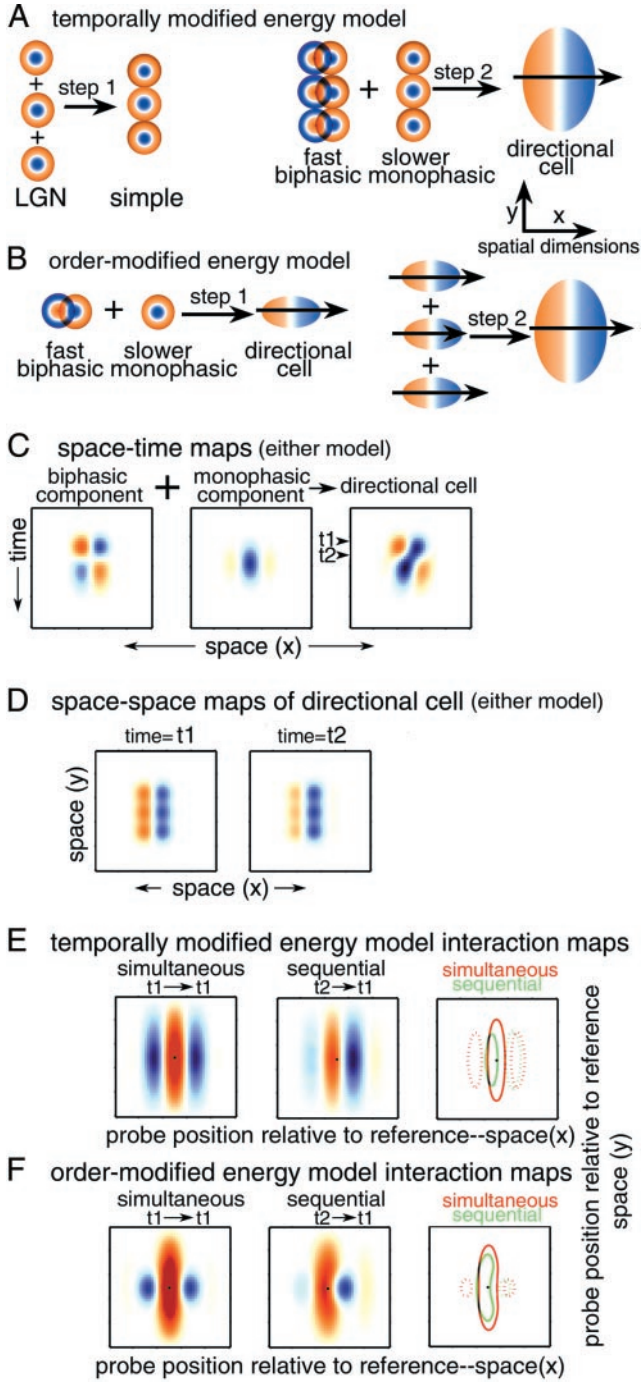

FIG. 9. Space/space/time model for the generation of a directional simple cell and its predicted interaction maps. See METHODS for model details. *A* and *B*: diagram of 2 possible sequences for generating a cell with both orientation and direction selectivity: orientation selectivity is generated before direction selectivity (conventional energy model, *A*) or direction selectivity is generated before orientation selectivity (*B*). In *A–D*, red indicates light excitation/dark suppression and blue indicates dark excitation/light suppression. In *E* and *F* red indicates facilitatory interactions and blue indicates suppressive interactions. See text for details.

Figure 9 (*A* and *B*), shows the distinction between direction selectivity being generated before or after receptive-field elongation. In *A*, *oriented*, spatiotemporally separable simple cells are combined to give an oriented, space-time-slanted, directional simple cell (as in the original energy model, Adelson and Bergen 1985). In *B*, *unoriented* spatiotemporally separable cells, such as LGN inputs or layer 4C cells, are combined to form unoriented directional cells, which are then combined in spatial alignment to form oriented directional cells. In *C* and *D*, we show the first-order maps of the nondirectional components and the combined, directional and oriented cells; *C* shows the first-order, space-time maps, and *D* shows first-order space-space maps. These first-order maps are identical for both versions of the model (*A* and *B*). That is, the first-order maps do not depend on the sequence of the generation of direction selectivity and receptive-field elongation. In *E* and *F* are shown the calculated interaction (2nd order) maps for pairs of light stimuli; the two models differ in these second-order maps because rectification of inhibition occurs at different stages in the two models.

As shown by Sakai and Tanaka (2000), the interaction maps for the first model (*E*) consist of alternating rows of facilitation and suppression that shift position over time but remain as parallel bands as previously observed for directional cells in cat V1 (Szulborski and Palmer 1990) and in monkey V1 (Gaska et al. 1994).

But this is not exactly what we observed in 2-D interaction maps of many macaque V1 directional cells. We observed either round-interaction maps or elongated maps with a distinct inflection at the origin. In model *B*, because inhibition rectifies, the suppression will act only locally, with each suppressive region interacting with only one of the three excitatory subunits. The interactions for the elongated directional cell (after step 2 in *B*) are shown in *F*, and indeed resemble the chevron-shaped 2-D interaction maps. Moreover, the cells generated after step 1 in model *B* would generate round interaction maps. Thus model *B* could generate both kinds of interaction maps that we actually observed, the round-interaction maps and the chevron-shaped maps. Thus we can reproduce a chevron-shaped interaction map by generating directionality before the stage of elongation of the receptive field. We could *not* reproduce the chevron shape in model *A* either by using different balances of ON and OFF inputs or by manipulating the spatial phases of the nondirectional components.

The distinction between the two models is not dramatic, however; and for the simultaneous interactions, the suppressive regions are slightly shorter than the facilitatory interactions even in model *A*. Therefore although our data look more consistent with model *B* than model *A*, the distinction is not clear enough for us to rule model *A* out. However, the presence of round complex-cell interactions and the existence of directional simple cells with receptive fields that are not elongated along the orientation axis support our proposal that direction selectivity can occur prior to receptive-field elongation.

DISCUSSION

We recorded from direction-selective cells in alert macaque V-1 and mapped 2-stimulus interactions (simultaneous and sequential) in two spatial dimensions. Cells showed preferred-

direction facilitation and null-direction suppression for same-contrast pairs of sequential stimuli and the reverse for pairs of opposite-contrast stimuli. The organization of the suppressive and facilitatory interactions closely correlates with the cells' actual direction tuning and thus can be used to infer mechanisms underlying direction selectivity. Some of the interaction maps, consisting either of pairs of round interactions or elongated chevron-shaped interactions, were not predicted by existing models for direction selectivity. How do we interpret the interaction maps and what do they reveal about direction selectivity?

Feedforward or Feedback? Subunit structure or contextual interactions?

Our intention was to explore interactions between pairs of spots to reveal underlying mechanisms of direction selectivity. Maps of interactions between pairs of stimuli have been variously interpreted as revealing features of the receptive fields of input cells (Livingstone et al. 2001; Movshon et al. 1978a; Ohzawa et al. 1997; Szulborski and Palmer 1990), dendritic calculations (Emerson et al. 1987), or contextual interactions (Kapadia et al. 2000). Paired-stimulus interactions show the nonlinearities that accrue in the generation of a cell's response properties. These interactions could represent the average receptive-field structure of immediately antecedent cells, or they could represent nonlinearities of cells more than one stage antecedent to the cell being recorded. Alternatively they could represent nonlinearities of dendritic compartments in the cell being recorded (Emerson et al. 1987). A third possibility is that they represent feedback influences (Kapadia et al. 2000).

Our maps were generated using stimulus ranges that covered and extended slightly beyond the activating region of the receptive field so all three of these interpretations could potentially explain our maps. Our maps show the alternating bands of facilitatory and suppressive interactions and inversion with inverting contrast that were observed in other studies aimed at revealing subunit structure. However, our bow-tie like simultaneous interaction patterns are remarkably similar in shape and comparable in scale to the maps of Kapadia et al. (2000), who interpreted their interactions as contextual—i.e., arising from the long-range horizontal connections known to exist in V1 complex cells (Gilbert and Wiesel 1979) or feedback from higher areas.

The contrast-sign dependence (Fig. 7) of the interactions mitigates against the feedback interpretation: interactions that are facilitatory between pairs of white stimuli or between pairs of black stimuli are suppressive between a white and a black stimulus. Such contrast-sign dependence indicates that the interactions must arise between inputs that have opposing responses to light and dark stimuli presented at the same location. Complex cells do not have opposing responses to light and dark stimuli, therefore the contrast-sign selective interactions we map must occur between inputs that precede the complex-cell stage. This requirement makes it very unlikely that the interactions arise from long-range intracortical connections or feedback from higher areas. Second, the interactions revealed by the same-minus-inverting calculation are restricted to interactions that are contrast-sign-specific, because interactions arising between inputs at or after the complex-cell stage should cancel out. The long-interval subtraction method, on the other hand, does not eliminate contrast-sign independent processes, but the similarity between the maps generated using the two calculations indicates that little of the interactions in the long-interval subtraction maps can be attributed to complex-to-complex cell interactions. A third reason for thinking that our maps reveal receptive-field subunit structure rather than feedback influences is that the interaction patterns in complex cells are smaller than their first-order receptive fields; they are of the same scale as the receptive fields and interaction maps of simple cells at the same eccentricity. We would expect contextual interactions to occur over a larger spatial scale because they should extend from outside a cell's receptive field to inside it. On the other hand, Kapadia et al. (2000) did not test contrast-sign dependency, so it is possible that the interactions they mapped in complex cells are not feedback, as they suggest, but feedforward, reflecting the subunit structure of antecedent simple cells. The fact that their "contextual" stimuli alone activated their cells, in some cases more strongly than the "center" stimulus, suggests that their "contextual" stimuli could have stimulated feedforward inputs instead.

What do the interaction maps say about how direction-selective receptive fields are generated? Although the elongated maps we observed (Fig. 3, *right*) are similar to what would be predicted for the energy model, the interaction maps are not completely consistent with what would be predicted if complex direction-selective cells are constructed from oriented, direction-selective simple cells. First, some of the cells showed round interactions, indicating that the direction-selectivity generating mechanism in these cells is not elongated along the axis perpendicular to the preferred-motion axis. Second, most maps that did show elongated interactions showed directional interactions that were more localized than the orientation interactions, suggesting that in these cells, direction selectivity and orientation selectivity are not inextricably linked. We expected to see parallel bands of alternating facilitatory and suppressive interactions slightly longer than the receptive field itself, because simple cells, as originally described, have parallel, elongated, alternating regions of mutually inhibitory ON and OFF subregions (Ferster 1988; Hubel and Wiesel 1962), and each position in each subregion would be expected to interact with every position in its own subregion and along all the other subregions (Fig. 1*D*). Inspection of the interaction maps indicates that the facilitatory interaction patterns do not simply shift on going from simultaneous to sequential stimulus pairs. Instead the facilitatory region bends. The fact that elongated facilitatory interactions correlated with narrow orientation tuning but not narrow direction tuning also is consistent with the hypothesis that orientation and direction tuning are independent.

One scenario that could result in suppressive interactions being more local than facilitatory interactions is if the suppressive interactions arise at a stage before receptive-field elongation; that is, if directional cells with elongated receptive fields were made up by aligning directional cells whose directionality is generated at an antecedent unoriented stage. The existence of directional simple cells with round subunits and the existence of round interaction patterns in some complex cells supports this idea. Suppressive interactions that are more localized than facilitatory interactions are what you would expect for a simple cell made up from several geniculate-like center-surround inputs, if the center-surround inputs rectify. The downstream

simple cell would show facilitatory interactions between pairs of spots even when the spots activate the centers of different unoriented cells (because excitation is not affected by rectification), but it could show suppressive interactions only if the pairs of spots activate the center and the surround of the same unoriented cell (because inhibition does rectify).

By considering the possibility that directionality is generated by a spatially offset inhibition and that this inhibitory interaction rectifies before orientation selectivity (receptive-field elongation), we can account for bowtie-shaped simultaneous interaction maps and both chevron-shaped and round sequential interaction maps. This model is equivalent to models that have been proposed previously but that do not explicitly deal with the dimension along the orientation axis. For example, it has been proposed that in the cat (Saul and Humphrey 1990) and monkey (DeValois et al. 2000), the two components in the energy model having different temporal properties could be accounted for by two populations of geniculate inputs, which differ in temporal properties. If the inputs to the first stage in generating direction selectivity are geniculate fibers, or geniculate-like, then direction selectivity would indeed arise before orientation selectivity.

The idea that directional interactions can precede receptive-field elongation is supported by some receptive-field maps of directional simple cells having a single round ON region adjacent to a round OFF region, as well as the existence of complex cells with round interaction maps. This further suggests that ON/OFF subregion organization can occur independently of the expansion of inputs along the orientation axis. Several studies in both cat and monkey have reported that many nondirectional simple cells are similarly not elongated along the orientation axis (Bullier et al. 1982; Pei et al. 1984; Ringach 2002).

An intermediate model might also be able to explain the chevron-shaped maps (although not the round maps). Jacobson et al. (1993) suggested that the nonlinearities apparent in the second-order maps of simple cells might reflect rectification of the inhibitory surround of LGN inputs. Thus even if alignment of unoriented inputs precedes the generation of direction selectivity, the rectification of LGN surrounds might result in more localized suppressive interactions than facilitatory interactions. But in this case, the suppressive interactions would not be expected to be directional, and our maps indicate that they are.

It is also possible that a cortical network could result in the interaction patterns we observed, but this network would have to retain contrast-sign selectivity, which is not characteristic of complex cells, so such networks would have to consist of simple cells. Because we can explain our observations with a feedforward mechanism, such a network explanation seems unnecessary.

D. Freeman developed all the computer programs and T. Chuprina provided excellent technical assistance. C. Pack, R. Born, and D. Tsao supplied useful and elegant software.

This work was supported by National Eye Institute Grant EY-13135 and P30 EY-12196.

REFERENCES

Adelson EH and Bergen JR. Spatiotemporal energy models for the perception of motion. *J Opt Soc Am A Opt and Image Sci* 2: 284–299, 1985.

Albright TD, Desimone R, and Gross CG. Columnar organization of directionally selective cells in visual area MT of the macaque. *J Neurophysiol* 51: 16–31, 1984.

Alonso JM, Usrey WM, and Reid RC. Rules of connectivity between geniculate cells and simple cells in cat primary visual cortex. *J Neurosci* 21: 4002–4015, 2001.

Anstis SM and Rogers BJ. Illusory reversal of visual depth and movement during changes of contrast. *Vis Res* 15: 957–961, 1975.

Anzai A, Ohzawa I, and Freeman RD. Neural mechanisms for processing binocular information. II. Complex cells. *J Neurophysiol* 82: 909–924, 1999.

Baker CL Jr. Linear filtering and nonlinear interactions in direction-selective visual cortex neurons: a noise correlation analysis. *Vis Neurosci* 18: 465–485, 2001.

Barlow HB and Levick WR. The mechanism of directionally selective units in rabbit's retina. *J Physiol* 178: 477–504, 1965.

Bullier J and Henry GH. Laminar distribution of first-order neurons and afferent terminals in cat striate cortex. *J Neurophysiol* 42: 1271–1281, 1979.

Bullier J, Mustari MJ, and Henry GH. Receptive-field transformations between LGN neurons and S-cells of cat striate cortex. *J Neurophysiol* 47: 417–438, 1982.

Conway BR. Spatial structure of cone inputs to color cells in macaque primary visual cortex (V-1). *J Neurosci* 21: 2768–2783, 2001.

Conway BR and Livingstone MS. Space-time maps and two-bar interactions of different classes of direction-selective cells in macaque V1. *J Neurophysiol* 89: 2726–2742, 2002.

De Valois RL, Cottaris NP, Mahon LE, Elfar SD, and Wilson JA. Spatial and temporal receptive fields of geniculate and cortical cells and directional selectivity. *Vis Res* 40: 3685–3702, 2000.

Emerson RC, Bergen JR, and Adelson EH. Directionally selective complex cells and the computation of motion energy in cat visual cortex. *Vis Res* 32: 203–218, 1992.

Emerson RC, Citron MC, Vaughn WJ, and Klein SA. Nonlinear directionally selective subunits in complex cells of cat striate cortex. *J Neurophysiol* 58: 33–65, 1987.

Ferster D. Spatially opponent excitation and inhibition in simple cells of the cat visual cortex. *J Neurosci* 8: 1172–1180, 1988.

Ferster D and Lindstrom S. An intracellular analysis of geniculo-cortical connectivity in area 17 of the cat. *J Physiol* 342: 181–215, 1983.

Gaska JP, Jacobson LD, Chen HW, and Pollen DA. Space-time spectra of complex cell filters in the macaque monkey: a comparison of results obtained with pseudowhite noise and grating stimuli. *Vis Neurosci* 11: 805–821, 1994.

Gilbert CG and Wiesel TN. Morphology and intracortical projections of functionally characterised neurones in the cat visual cortex. *Nature* 280: 120–125, 1979.

Goodwin AW and Henry GH. Direction selectivity of complex cells in a comparison with simple cells. *J Neurophysiol* 38: 1524–1540, 1975.

He S and Masland RH. Retinal direction selectivity after targeted laser ablation of starburst amacrine cells. *Nature* 389: 378–382, 1997.

Heeger DJ. Half-squaring in responses of cat striate cells. *Vis Neurosci* 9: 427–443, 1992.

Hirsch JA, Alonso JM, Reid RC, and Martinez LM. Synaptic integration in striate cortical simple cells. *J Neurosci* 18: 9517–9528, 1998.

Hoffman KP and Stone J. Conduction velocity of afferents to cat visual cortex: a correlation with cortical receptive field properties. *Brain Res* 32: 460–466, 1971.

Hubel DH. Tungsten microelectrode for recording from single units. *Science* 125: 549–550, 1957.

Hubel DH and Wiesel TN. Receptive fields, binocular interaction and functional architecture in the cat's visual cortex. *J Physiol* 160: 106–154, 1962.

Jacobson LD, Gaska JP, Chen H-W, and Pollen DA. Structural testing of multi-input linear-nonlinear cascade models for cells in macaque striate cortex. *Vis Res* 33: 609–626, 1993.

Kapadia MK, Westheimer G, and Gilbert CD. Spatial distribution of contextual interactions in primary visual cortex and in visual perception. *J Neurophysiol* 84: 2048–2062, 2000.

Kontsevich LL. The nature of the inputs to cortical motion detectors. *Vis Res* 35: 2785–2793, 1995.

Livingstone MS. Mechanisms of direction selectivity in macaque V1. *Neuron* 20: 509–526, 1998.

Livingstone MS, Pack CC, and Born RT. Two-dimensional substructure of MT receptive fields. *Neuron* 30: 781–793, 2001.

Livingstone MS and Tsao DY. Receptive fields of disparity-selective neurons in macaque striate cortex. *Nat Neurosci* 2: 825–832, 1999.

Martin KA and Whitteridge D. Form, function and intracortical projections of spiny neurones in the striate visual cortex of the cat. *J Physiol* 353: 463–504, 1984.

Mel BW, Ruderman DL, and Archie KA. Translation-invariant orientation tuning in visual "complex" cells could derive from intradendritic computations. *J Neurosci* 18: 4325–4334, 1998.

Movshon JA, Thompson ID, and Tolhurst DJ. Receptive field organization of complex cells in the cat's striate cortex. *J Physiol* 283: 79–99, 1978a.

Movshon JA, Thomson ID, and Tolhurst DJ. Spatial summation in the receptive fields of simple cells in the cat's striate cortex. *J Physiol* 283: 53–77, 1978b.

Ohzawa I, DeAngelis GC, and Freeman RD. Stereoscopic depth discrimination in the visual cortex: neurons ideally suited as disparity detectors. *Science* 249: 1037–1041, 1990.

Ohzawa I, DeAngelis GC, and Freeman RD. Encoding of binocular disparity by complex cells in the cat's visual cortex. *J Neurophysiol* 77: 2879–2909, 1997.

Pie X, Vidyasagar TR, Volgushev M, and Creutzfeld OD. Receptive field analysis and orientation selectivity of postsynaptic potentials of simple cells in cat visual cortex. *J Neurosci* 14: 7130–7140, 1994.

Ringach DL. Spatial structure and symmetry of simple-cell receptive fields in macaque primary visual cortex. *J Neurophysiol* 88: 455–463, 2002.

Robson JG. Spatial and temporal contrast-sensitivity functions of the visual system. *J Opt Soc Am* 56: 1141–1142, 1966.

Rybicki GB, Tracy DM, and Pollen DA. Complex cell response depends on interslit spacing. *Nat New Biol* 240: 77–78, 1972.

Sakai K and Tanaka S. Spatial pooling in the second-order spatial structure of cortical complex cells. *Vis Res* 40: 855–871, 2000.

Saul AB and Humphrey AL. Spatial and temporal response properties of lagged and nonlagged cells in cat lateral geniculate nucleus. *J Neurophysiol* 64: 206–224.

Schiller PH, Finlay BL, and Volman SF. Quantitative studies of single-cell properties in monkey striate cortex. I. Spatiotemporal organization of receptive fields. *J Neurophysiol* 39: 1288–1319, 1976.

Szulborski RG and Palmer LA. The two-dimensional spatial structure of nonlinear subunits in the receptive fields of complex cells. *Vis Res* 30: 249–254, 1990.

Tanaka K. Cross-correlation analysis of geniculostriate neuronal relationships in cats. *J Neurophysiol* 49: 1303–1318, 1983.